

## RESEARCH ARTICLE

# Numerical simulation of the boundary layer development behind a single quarter elliptic-wedge spire

M. A. Fitriady<sup>1,3\*</sup>, N. A. Rahmat<sup>1</sup>, A. F. Mohammad<sup>2</sup>, and S. A. Zaki<sup>2</sup>

<sup>1</sup> Faculty of Technology Mechanical and Automotive Engineering, Universiti Malaysia Pahang (UMP), 26600, Pahang, Malaysia  
Phone: +6094315017

<sup>2</sup> Malaysia-Japan International Institute of Technology, Universiti Teknologi Malaysia (UTM), 54100, Kuala Lumpur, Malaysia

<sup>3</sup> Research Center for Chemistry, Nasional Research and Innovation Agency (BRIN), 15314, Banten, Indonesia

**ABSTRACT** - For decades wind tunnel has been utilized to generate a quasi-atmospheric boundary layer to observe the wake flow around objects submerged within the Atmospheric Boundary Layer. The quarter elliptic-wedge spire is the most commonly used as a vortex generator among other passive devices. However, despite numerous past studies that utilize rows of spires to generate deep quasi-ABL, only a few researchers targeted spires as the main subject of their investigation. Hence, the present work originally aims to investigate the wake flow structure behind a single quarter elliptic-wedge spire and its aerodynamic interaction with a smooth wall boundary layer. A computational fluid dynamics simulation predicting the wake flow structure behind a single quarter elliptic-wedge spire was conducted using the OpenFOAM® software. The computational domain consists a smooth flat plate, and a single quarter elliptic-wedge spire. A comparison of two Reynolds-Averaged Navier–Stokes turbulence models, namely the  $k-\varepsilon$  model and the SST  $k-\omega$  model, was conducted. A SIMPLE algorithm was used as the solver in the simulation iteration and ParaFOAM® was used as the post-processing software. The development of the boundary layer height from streamwise  $x_0=0.5S$  to downwind  $x_0=20S$  was observed. The mean vertical velocity profiles predicted by both turbulence models are in good agreement with the previous wind tunnel experimental results. However, the results obtained with the  $k-\varepsilon$  model were overpredicted compared to the results of the SST  $k-\omega$  model causing deviation of the boundary layer height from the wind tunnel experimental data. This anomaly might be caused by the velocity deficit recovery above the boundary layer height region where the turbulence is low.

## ARTICLE HISTORY

Received : 26th July 2022

Revised : 11<sup>th</sup> May 2023

Accepted : 18<sup>th</sup> May 2023

Published : 28<sup>th</sup> June 2023

## KEYWORDS

Computational fluid dynamic

Spire

Wake flow

$k-\varepsilon$

SST  $k-\omega$

## 1.0 INTRODUCTION

For decades, numerous field studies observed the aerodynamic responses of vehicles and buildings that were fully immersed in the Atmospheric Boundary Layer (ABL) by submerging the small-scaled model into the ABL [1–3]. However, it is difficult to observe these responses in the real ABL due to non-control conditions where all properties need to be considered, including temperature. Alternatively, researchers especially from wind engineering and urban climate fields generate a quasi-ABL in a more controlled condition, i.e. a boundary layer wind tunnel (BLWT). Even though it is possible to recreate quasi-ABL inside the BLWT, the required test section length to generate a fully developed quasi-ABL that imitates the real ABL is enormous, typically 20-30 meters [4, 5]. Hence, a man-made device, namely a vortex generator was introduced to enhance the depth of the quasi-ABL by intensifying the turbulent flow inside the wind tunnel [6–10].

Two methods have been widely practised to generate quasi-ABL in the wind tunnel experiment, namely the active and passive approaches [10, 11]. Despite its excellent role in enhancing the boundary layer depth inside the wind tunnel, active approaches are considered very costly to be applied in common practice [5]. Hence, the cost-effective passive approach is commonly utilised by installing a row-set of vortex generators [12] in the upwind section of the BLWT. Between several vortex generators designs, such as triangular, triangular with splitter plate, or plane elliptic, the quarter elliptic-wedge spire [11] is the most widely used in the wind tunnel experiment due to its ability to generate a symmetric, constant, deep enough boundary layer in the limited streamwise distance [6, 11, 13].

Numerous studies have utilized the quarter-elliptic wedge spire as the vortex generator to generate deep quasi-ABL. Hagishima *et al.* (2009) and Zaki *et al.* (2011 & 2012) used a set of quarter elliptic-wedge spires as a vortex generator to identify the measured drag coefficient ( $C_d$ ) which is produced by the rough walls consisting of cubes in the furious pattern of arrangement [14–16]. Kozmar (2016 & 2019) used a set of quarter elliptic-wedge spires completed with the castellated barrier wall as a vortex generator followed by the roughness wall consisting of arranged cubes to observe the wind turbine wake downwind of a mountain [17, 18].

Despite numerous past studies that utilize rows of spires to generate deep quasi-ABL, most of the experiments were studying more of the effect of the roughness element rather than the spire [14, 15, 19]. Only a few researchers targeted spires as the main subject of their investigation [6, 7, 20, 21], hence, the flow structure behind these vortex generators is not yet fully understand. This fact indicates a research gap in investigating the wake flow structure behind the spire and its aerodynamic interaction with the developing wall boundary layer in the wind tunnel. On the other hand, the utilization of Computational Fluid Dynamics (CFD) in the wind engineering field has seen growth in the last few decades. Numerous CFD studies have been conducted to investigate the wake flow behind the structure [3, 22–24]. This method supports the wind tunnel experiment due to its ability to observe the flow structure much further downstream where it is limited in the wind tunnel experimental studies.

The present work originally aims to investigate the wake flow structure behind a single quarter-elliptic wedge spire and its aerodynamic interaction with a smooth wall boundary layer based on CFD. Two Reynolds-Averaged Navier Stokes (RANS) turbulence models, i.e.  $k-\epsilon$  and  $SST k-\omega$  models, were applied and compared in terms of result accuracy relative to the wind tunnel experimental data from the published work. However, we found discrepancies in BLH results between these two turbulence models. Hence, the present paper focused on discussing vertical velocity profiles and developing the boundary layer from upwind to further downwind. The findings from this work contribute to the existing literature with an improved understanding of the flow behind the spire.

## 2.0 METHODOLOGY

This study was conducted using open-source CFD software, OpenFOAM®. The preparation for the CFD consists of the numerical domain creation and the setup of the turbulence model and time step. Upon the execution, *simpleFoam* was used as the solver of the simulation. Finally, post-processing, including data extraction and data analysis, was conducted using ParaView®.

### 2.1 Numerical Domain

The numerical domain consists of the wind tunnel model, the flat plate model, and the spire model. The wind tunnel has a dimension of 0.3 m (height) × 0.3 m (width) × 3 m (streamwise length). The flat plate was included in the simulation based on the wind tunnel study [7]. Moreover, the spire model has a quarter elliptical shape as used in the previous study [11]. It has a height of 0.05 m ( $S$ ), a length of 0.025 m ( $0.5S$ ), and a width of 0.005 m ( $0.1S$ ). The wedge angle is  $5.71^\circ$  by default. Based on the previous wind tunnel study [7], the spire was installed at the upwind position in the center of the wind tunnel,  $2S$  from the leading edge of the flat plate. Figure 1 presents the layout of the computational domain based on the previous wind tunnel study layout completed with the dimension of the spire [7]. To highlight the effect of the spire, two conditions were applied to this study, i.e. without any spire installed (WO) and with a single spire installed (WS).

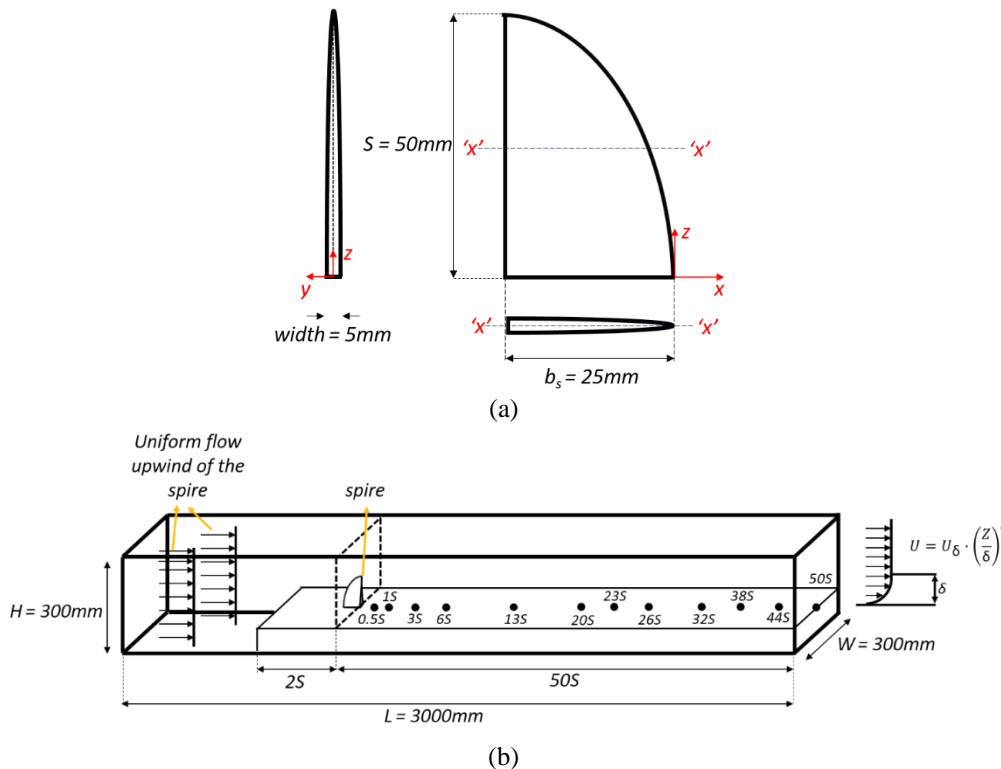


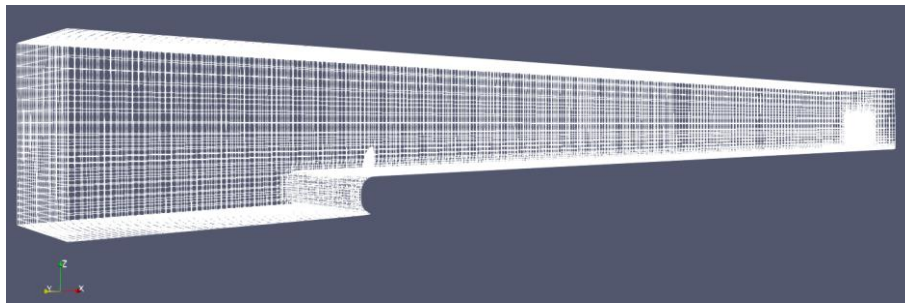
Figure 1. Schematic of (a) a quarter elliptic-wedge spire model and its dimension, and (b) the layout of the computational domain completed with the flat plate and the spire

To observe the development and the recovery of the wake flow, the distribution of streamwise velocity was measured at twelve leeward positions from the near wake regions of  $x_0=0.5S$ ,  $1S$ ,  $3S$ , and  $6S$  to far wake regions of  $x_0=13S$ ,  $20S$ ,  $26S$ ,  $32S$ ,  $38S$ ,  $44S$ , and  $50S$  for both WO and WS cases. In addition, the vertical velocity profile was measured from  $z_0=0.0002$  m ( $0.004S$ ) above the flat plate up to  $z_0=0.23$  m ( $4.6S$ ) in the vertical direction. To summarize the variable, Table 1 presents all the CFD variable conditions observed in this study.

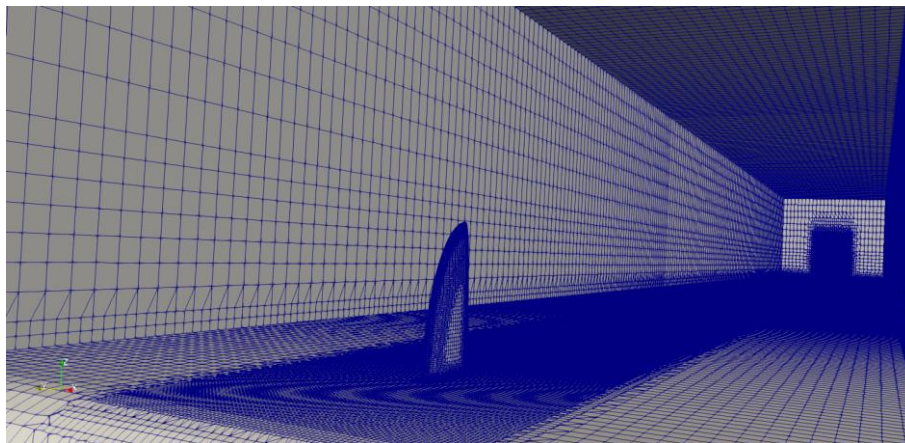
The 3D model is designed using open-source Computer-Aided Design (CAD) software i.e. FreeCAD®. Both the *blockMesh* utility and the *snappyHexMesh* utility were used to finalize the numerical domain. The mesh generation was initialized by *blockMesh* utility for creating the basic wind tunnel rectangular shape numerical domain. While the *snappyHexMesh* utility was used to incorporate the flat plate completed with the spire into the basic rectangular numerical domain. A refinement box was created on both sides and above the spire along with the streamwise direction with the level of refinement of 3. In addition, a refinement surface was applied for the spire with a level of refinement of 10. Using these configurations, a numerical domain with cell numbers of 10 million and 11 million was generated for WO and WS cases, respectively. More than 95% of the cells are hexahedra while the rest are polyhedra. Figure 2 shows the wire mesh view of the numerical domain and the 3-D spire model inside the domain.

Table 1. The CFD variable condition

	Near wake region	Far wake region
WO and WS	Streamwise direction ( $x_0$ ) = $0.5S$ , $1S$ , $3S$ , and $6S$	Streamwise direction ( $x_0$ ) = $13S$ , $20S$ , $26S$ , $32S$ , $38S$ , $44S$ , and $50S$
Turbulence model $k-\varepsilon$ and $SST k-\omega$	Vertical direction ( $z$ ): $0.004S - 4.6S$	



(a)



(b)

Figure 2. The numerical domain for the CFD: (a) The wire mesh view of the domain and (b) The internal view of the domain showing the 3-D quarter elliptic-wedge spire model

## 2.2 Turbulence Model and Time Step Setting

The simulations were carried out using a two-equation turbulence model the Reynolds-Averaged Navier Stokes (RANS) including both the  $k-\varepsilon$  and  $SST k-\omega$  models. This model was selected because the RANS turbulence model requires a lower computational load compared to the Large Eddy Simulation (LES) [25]. On top of that, the simulation of ABL generation inside a wind tunnel case study using this turbulence model produced a good and representable result [26–28]. The following initial conditions were applied; incoming flow speed ( $U=10$  ms<sup>-1</sup>), the turbulence dissipation rate constant ( $\varepsilon=14.855$  m<sup>2</sup>s<sup>-3</sup>), and the specific turbulence dissipation rate constant ( $\omega=440.148$  s<sup>-1</sup>). The simulations were run in parallel using eight processors with the time step of 1s. The data was written and recorded every 50-time steps. The simulations were executed with the steady-state solver, *simpleFoam*.

The computation reached a steady state condition when the convergence point is achieved. However, in this study case, it cannot be achieved because some of the residual values are always above the tolerance and tend to be constant. Hence, the convergence points were determined based on the residual chart pattern. The residual chart can be seen in Figure 3.

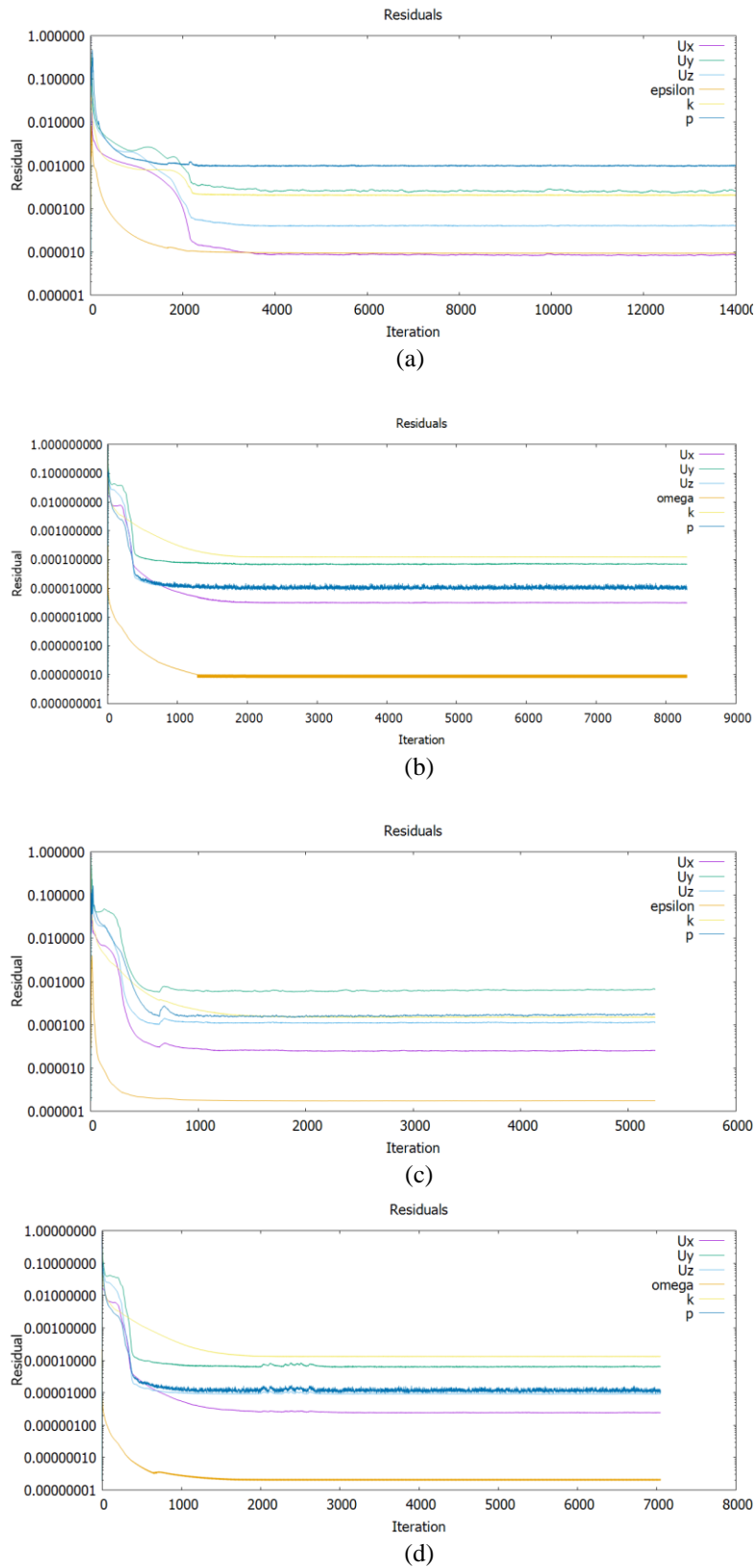


Figure 3. Residual plot for each case: (a) WO  $k-\epsilon$ , (b) WO SST  $k-\omega$ , (c) WS  $k-\epsilon$ , and (d) WS SST  $k-\omega$

Based on the residual chart it can be stated that all cases are already in a steady state at 5000 iterations. Hence, the data used in the discussion is at the latest timestep.

### 2.3 Data Acquisition and Analysis

The vertical velocity profile was extracted using the post-processing software, ParaFOAM®. The numerical domain was sliced based on the distance in the streamwise direction ( $x_0$ ) from  $x_0=0.5S$  up to  $x_0=50S$ , and then plotted over the line vertically in the centre ( $y=0$ ) of the spanwise direction. The data were extracted for the last time steps using the save data feature. The analyses include a graphical plot, and the discussion was presented based on these analyses.

## 3.0 RESULTS AND DISCUSSION

To compare the turbulence models, the results obtained from the two cases, WO and WS, are analysed and presented in this section. This is followed by a discussion of the results of the boundary layer height (BLH) analysis.

### 3.1 Without Spire Case

#### 3.1.1 Mean vertical velocity profile

Figure 4 presents the mean vertical velocity profile at the centre of the lateral direction ( $y=0$ ) of both  $k-\epsilon$  and  $SST\ k-\omega$  turbulence models for the WO case.  $U/U_{ref}$  is the streamwise velocity ( $U$ ) normalized by the reference velocity ( $U_{ref}$ ) at  $y=0$  and  $z=2S$  for each streamwise position. The wind tunnel experimental data was included for comparison [6, 7].

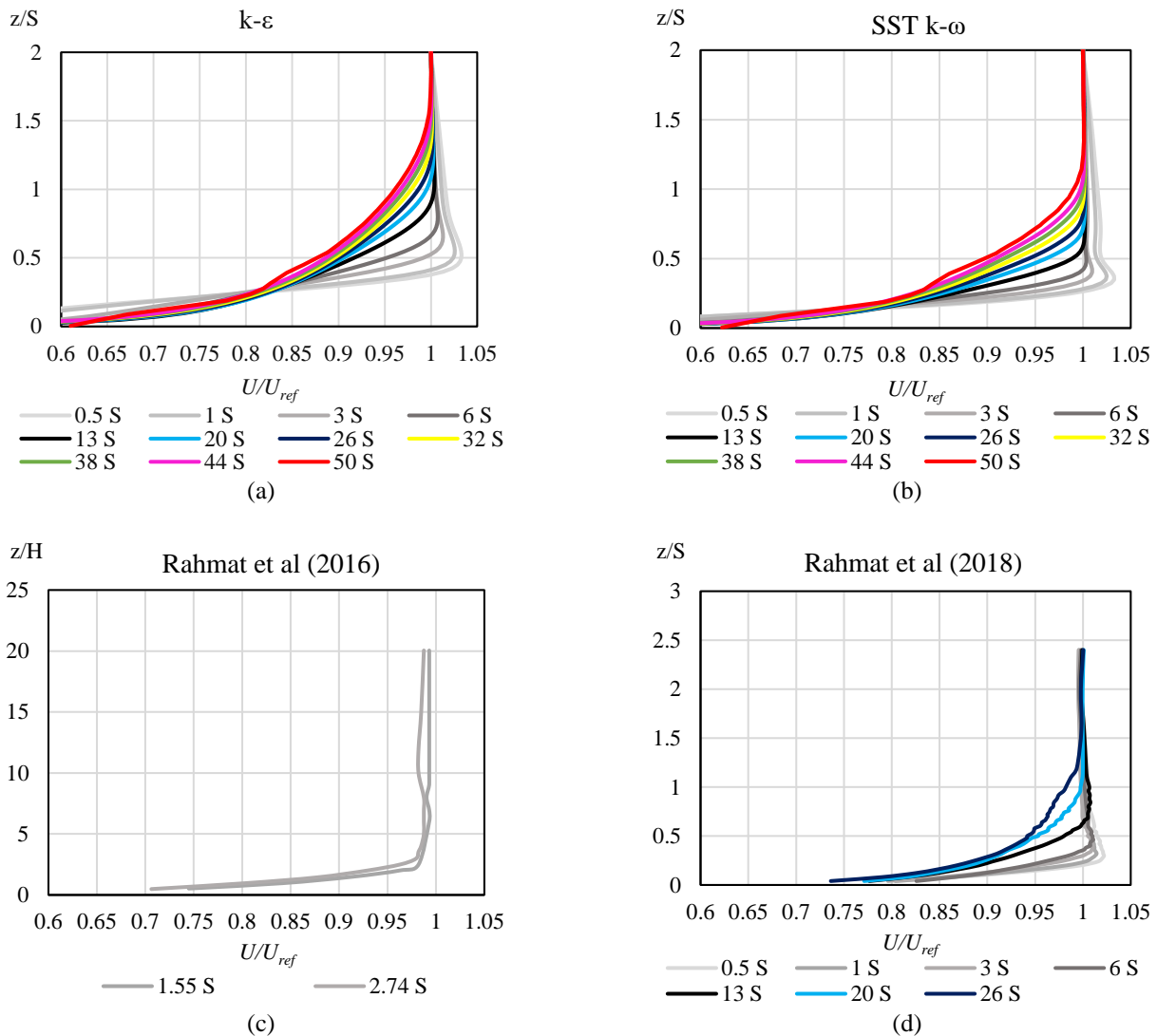


Figure 4. Normalized vertical velocity profiles at the center point of the wind tunnel of WO case for; (a)  $k-\epsilon$  turbulence model and (b)  $SST\ k-\omega$  turbulence model. The wind tunnel experimental data: (c) Rahmat *et al.* (2016) and (d) Rahmat *et al.* (2018), were also included for comparison [6, 7]. The vertical axis indicates the elevation normalized by the spire height,  $S$

The mean vertical velocity profiles for the  $k-\epsilon$  and  $SST k-\omega$  turbulence models are shown in Figure 4(a) and 4(b), respectively. Both profiles are similar to each other. The normalized velocity is at the lowest value just above the smooth wall due to the drag coefficient and logarithmically increased as the vertical distance increased. The drag coefficient weakens as the vertical distance increases. Hence, at some point, the drag coefficient is very small that it is neglected i.e. normalized velocity equal to one. Moreover, the normalized velocity reached the highest value at the near wake region i.e.  $x_0=0.5S, 1S, 3S,$  and  $6S$  on the vertical distance of  $0.5S$  and  $0.3S$  for  $k-\epsilon$  and  $SST k-\omega$  respectively. This phenomenon might be caused by turbulence generation due to the leading edge of the smooth plate.

On top of that, the changes in the velocity gradient in the profiles are increasing along with the streamwise distance. These phenomena indicate the development of the BLH as the streamwise distance increases for both turbulence models. The velocity profiles are close to unity above the height of  $z=1S$  and  $z=1.5S$  for the  $SST k-\omega$  model and  $k-\epsilon$  model, respectively. This shows the overprediction of the  $k-\epsilon$  model compared to the  $SST k-\omega$  model. The mean vertical velocity profile and the development of the BLH are in good agreement with [6, 7], while the highest normalized velocity value presented in this study is also observed in [7].

Based on the previous study [6, 7, 14], the height of the negative peak of the skewness profile of the vertical velocity can be determined as the BLH. However, since this is a steady-state case, the fluctuation of the vertical velocity based on the time step cannot be observed. Another method to determine the BLH is proposed by Kozmar et al. who stated that the BLH is the height where the vertical velocity equals 99.9% of the freestream [29, 30]. In this study, the BLH is determined using the method proposed by Kozmar et al. The BLH are discussed later in this chapter.

### 3.1.2 Mean vertical velocity in different stream-wise positions

The mean vertical velocity profiles at several points in a streamwise direction are shown in Figure 5, to highlight the overprediction of the  $k-\epsilon$  model compared to the  $SST k-\omega$  model. The wind tunnel experimental data were also included for the distance of  $1S$  and  $6S$  as a comparison. The vertical velocity predicted by the turbulence model for the near wake region, namely  $x_0=1S$  and  $x_0=6S$ , is in good agreement with the experimental data, especially the  $SST k-\omega$ . The overprediction can be observed, and the normalized velocity gradually increased as the distance in the streamwise direction increased. However, the basic shapes of the profiles are similar to each other.

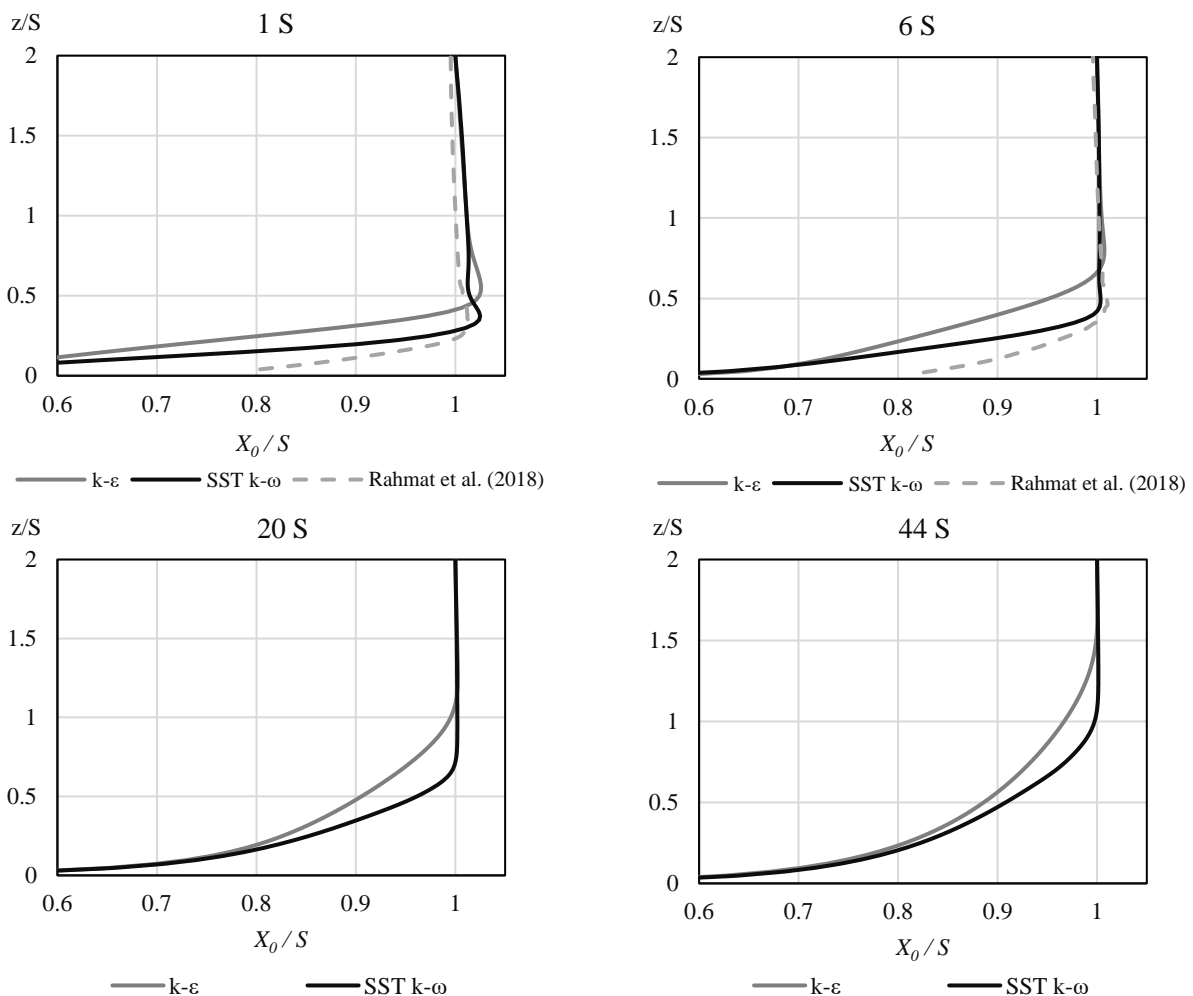


Figure 5. Mean vertical profiles of the  $k-\epsilon$  and  $SST k-\omega$  models at several streamwise positions, namely,  $x_0=1S, 6S, 23S,$  and  $44S$  for the WO case

This phenomenon might be caused by slight differences between the  $k-\varepsilon$  model and the  $SST k-\omega$  model. Generally, the  $k-\varepsilon$  model and  $k-\omega$  model are the same turbulence model. The turbulence dissipation rate ( $\varepsilon$ ) can be converted to the specific turbulence dissipation rate ( $\omega$ ) by using Eq. (1) [31, 32].

$$\omega = \frac{\varepsilon}{C_\mu k} \tag{1}$$

However, it is well known that the standard  $k-\varepsilon$  turbulence model poorly represents the separation flow due to the over-prediction of the turbulent kinetic energy in the stagnation points [33–35]. This is because of the damping of  $\varepsilon$  near the wall. Hence, the damping function has to be introduced to enhance the performance of this model, especially on the flow prediction in the near-wall regions [36]. On the contrary, the  $k-\omega$  model performs well in the flow prediction near-wall region because it does not need the damping function [37].

Based on the current study, the separation flow occurred in the near wake region close to the spire. Hence, it can be stated that the  $k-\omega$  model predicts more accurately in the near wake region while the  $k-\varepsilon$  model predicts more accurately in the far wake region. The  $SST k-\omega$  model was developed by combining the advantages of both the  $k-\varepsilon$  model and the  $k-\omega$  model. Hence, theoretically, the  $SST k-\omega$  turbulence model can predict accurately for both near and far wake regions.

### 3.2 With Spire Case

#### 3.2.1 Mean vertical velocity profile

Figure 6 presents the mean vertical velocity profiles at the center of the lateral direction ( $y=0$ ) for both  $k-\varepsilon$  and  $SST k-\omega$  turbulence models for the WS case.  $U/U_{ref}$  is the streamwise velocity ( $U$ ) normalized by the reference velocity ( $U_{ref}$ ) at  $y=0$  and  $z=2S$  for each streamwise position. Based on these figures, both turbulence models predict a similar normalized velocity profile for the far wake region which is the same as the WO case, i.e. Figure 4(a) and 4(b). Moreover, the overprediction of  $k-\varepsilon$  is also apparent.

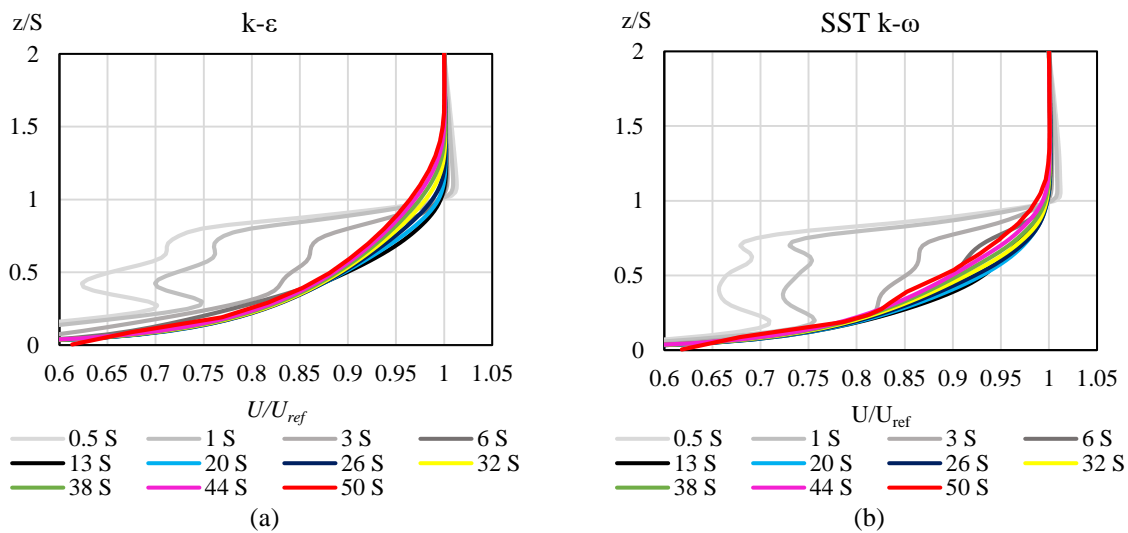


Figure 6. Normalized vertical velocity profiles at the center point of the wind tunnel of WS case for: (a)  $k-\varepsilon$  turbulence model and (b)  $SST k-\omega$  turbulence model. The vertical axis indicates the elevation normalized by the spire height,  $S$

On the other hand, based on the same figure, the two turbulence models predict the profile differently in terms of the shape of the fluctuation in the normalized vertical velocity profile. However, both turbulence models predict the fluctuation at the same near wake region; i.e.  $x_0=0.5S, 1S$ , and  $3S$

Moreover, the changes in the velocity gradient in the profile, which indicates the development of the BLH, are also observed in the far wake region only. While in the near wake region, there is an anomaly in the normalized vertical velocity profile for both turbulence models, which indicates that the BLH is decreasing instead of increasing as the streamwise distance increases. As explained in the introduction above, a row of spires is widely used in the wind tunnel experiment due to its ability to generate a symmetric, constant, deep enough boundary layer in the limited streamwise distance of the wind tunnel [6, 11, 13]. However, the results obtained from both turbulence models in the near wake region ( $x_0=0\sim 6S$ ) shown in Figure 6 contradict this statement. This is due to the current study only utilising a single quarter elliptic-wedge spire instead of a row of spires (around 5 to 6 spires installed in series) [11] which is insufficient to create turbulence to achieve the deep boundary layer in the wind tunnel.

#### 3.2.2 Mean vertical velocity in different stream-wise positions

To highlight the contrast between the  $k-\varepsilon$  model and the  $SST k-\omega$  model in the WS case, the mean vertical velocity profiles obtained at the  $x_0=1S, 6S, 20S$ , and  $44S$  are shown in Figure 7. The fluctuation in the normalized vertical velocity

profile obtained by the  $k-\varepsilon$  model is different in terms of shape, compared to the  $SST k-\omega$  model. However, the magnitude is still similar. The overprediction is still apparent, especially in the far wake region.

### 3.2.3 Vertical velocity profile of WO and WS case

The mean vertical velocity profiles of the WO and WS case predicted by both turbulence models at the near wake region were presented in Figure 8. The profile for vertical distance higher than  $1S$  for WS is the same as the WO case. However, the profile of the low-valued normalized velocity is distinctively different. The normalized velocity is at the lowest value just above the smooth wall and increased up to the vertical distance of  $1S$  creating a certain fluctuation. This low-valued normalized velocity fluctuation is the indication of the wake flow generated due to the spire. The effect of the wake flow weakens as the vertical distance increases. Hence, at the height above  $1S$ , the wake flow effect was very small that can be neglected.

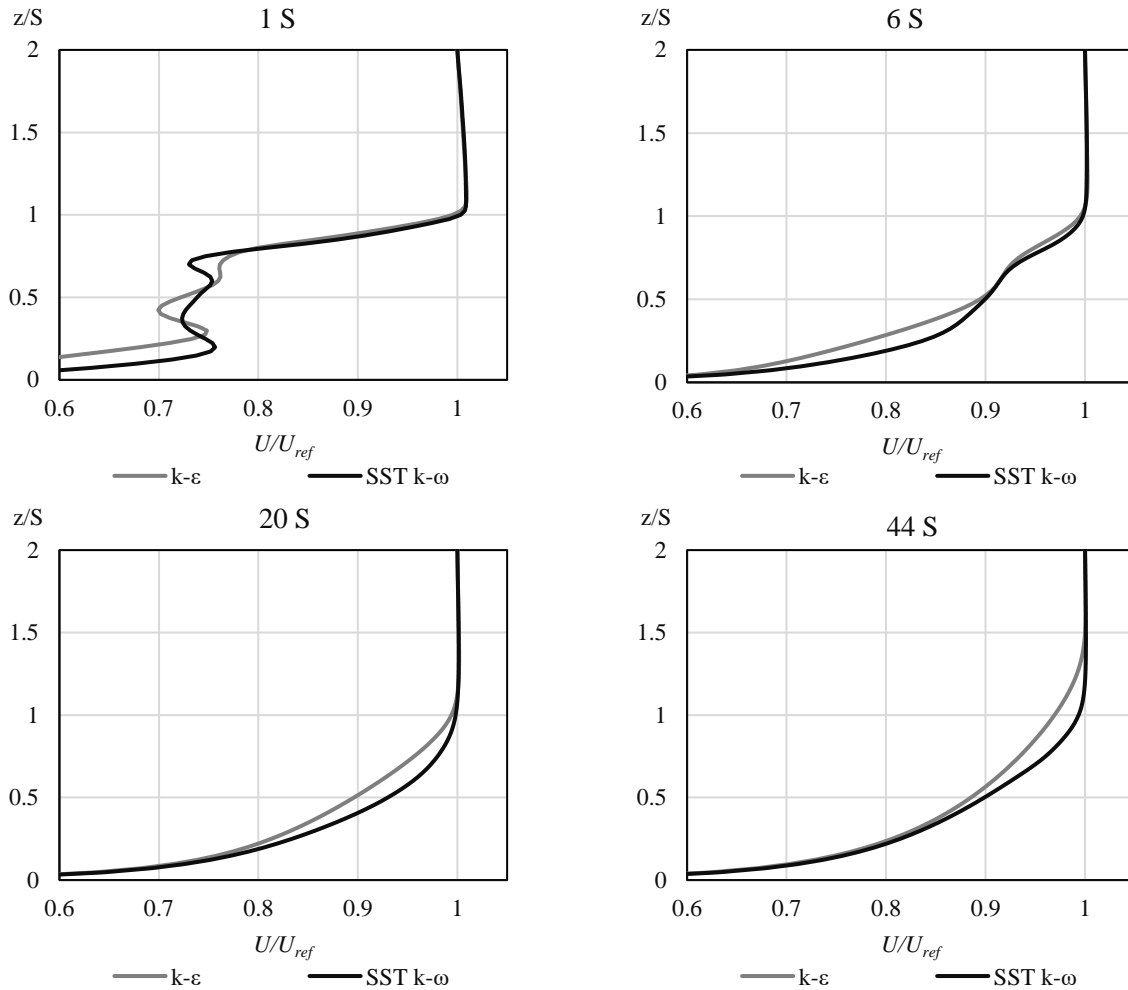


Figure 7. The mean vertical profiles of the  $k-\varepsilon$  model and  $SST k-\omega$  model at the streamwise locations of  $x_0=1S$ ,  $6S$ ,  $23S$ , and  $44S$  for the WS case

Moreover, the change of gradient velocity for the WS case is decreasing as the streamwise distance increases which can be observed in the mean vertical velocity profiles of both turbulence models. This is the indication of BLH reduction at the near wake region of the WS case. On the contrary, the change of gradient velocity for the WO case is increasing as the streamwise distance increases which implies that the BLH is developing as the streamwise distance increases.

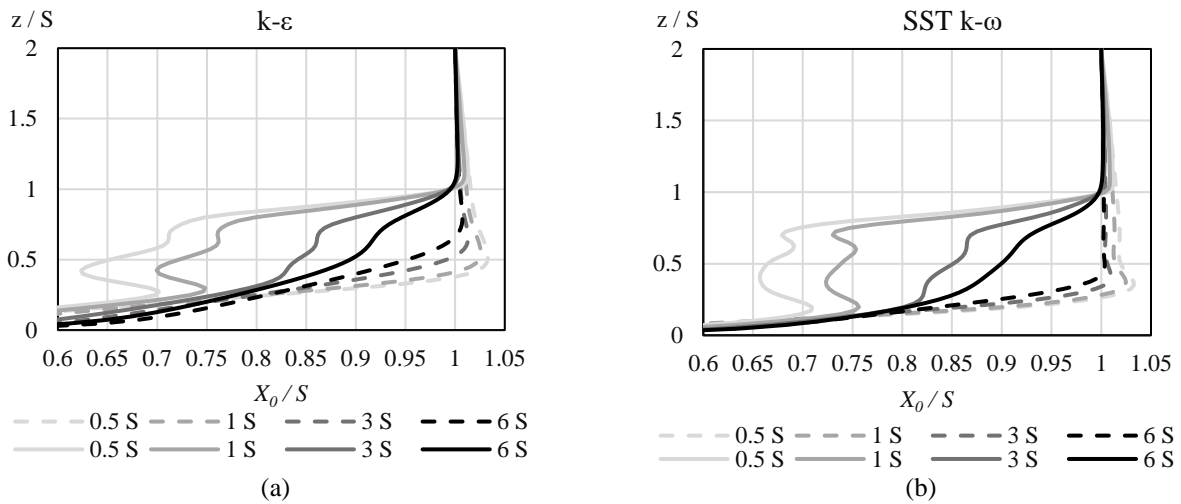


Figure 8. The vertical velocity profiles of the: (a) WO and (b) WS cases predicted by both turbulence models at the near wake region

### 3.3 Boundary-Layer Height

The BLH is determined by the height where the mean vertical velocity is equal to 99.9% of the freestream velocity ( $U/U_{ref}=0.999$ ) [29, 30]. The BLH predicted by the  $k-\epsilon$  and  $SST k-\omega$  turbulence models for both WO and WS cases can be seen in Figure 9(a) and Figure 9(b), respectively. The wind tunnel experimental data as well as previous studies [7, 20] are also included as a comparison.

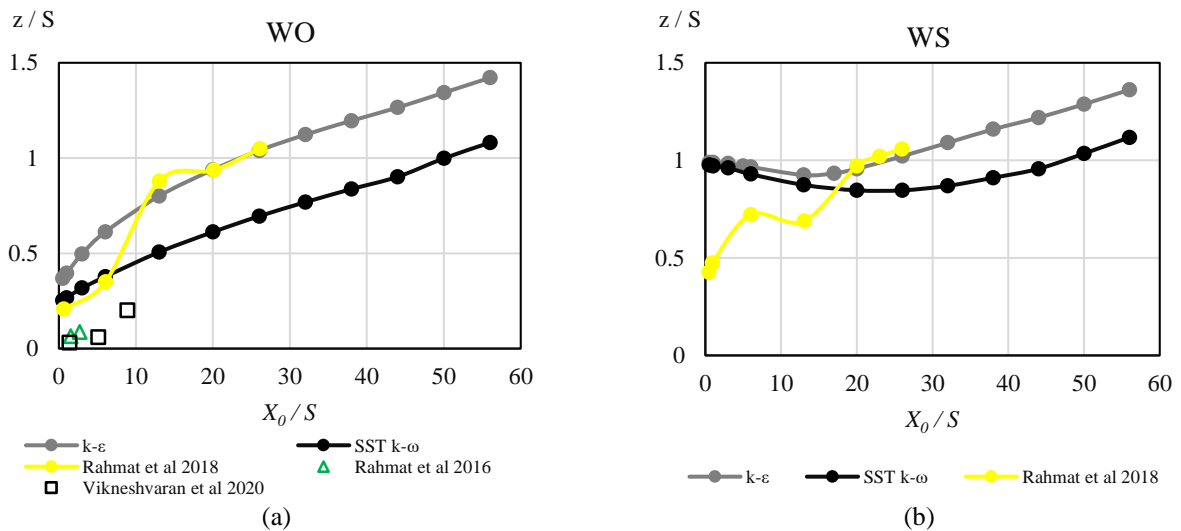


Figure 9. BLH development with streamwise distance using the  $k-\epsilon$  and  $SST k-\omega$  turbulence models for: (a) WO and (b) WS cases. The wind tunnel experimental data as well as previous studies are also included as a comparison. (Depicted from [8] and [7])

Based on Figure 9(a), it can be stated that the BLH in the WO case is developed with the increase of the streamwise distance for both  $k-\epsilon$  and  $SST k-\omega$  turbulence models. Moreover, the overprediction of  $k-\epsilon$  compared to the  $SST k-\omega$  turbulence model is also apparent. On the other hand, based on Figure 9(b), the BLH in the near wake region for the WS case slightly decreased down to a streamwise distance of  $x_0=13S$  and  $x_0=20S$  with a decrement of 6.5% and 13.2% for the  $k-\epsilon$  model and  $SST k-\omega$  model respectively, as discussed above that the current study only utilised a single spire instead of a row of spires to generate deep BLH. Then BLH profile gradually increased as the streamwise distance increased with an increment of 39.3% and 22.3% compared to the lowest point for  $k-\epsilon$  model and  $SST k-\omega$  model respectively. Moreover, Rahmat et al 2018 reported that the BLH decreased in the WS case from the streamwise distance of 6S down to 13S with a total decrement of 4.6% then it rose as the streamwise distance increased up to the highest point at 26S with the total increment of 53.7%. In other words, both numerical simulation and wind tunnel experiments present a similar decreasing pattern in the near wake region. This phenomenon might be caused by the velocity deficit recovery that occurs above the reference BLH, i.e. outer layer region with less wall effect and turbulence are relatively low [6].

Furthermore, Figure 10 presents the graphs of BLH predicted using the two turbulence models for both WO and WS cases. Based on Figure 10(a), it can be stated that in the  $k-\epsilon$  model simulation, the BLH of the WS case is deeper compared to the WO case by 250 % at  $x_0=0.5S$ . However, the BLH of the WS case decreased along with the streamwise distance in

the near wake region ( $x_0=0\sim 6S$ ). At around  $x_0=13S$ , the BLH of the WS case reached the minimum point and starts to develop as the distance in the streamwise direction increased. Even though the BLH of the WS case is slightly shallower compared to the WO case, the difference between them is insignificant. In other words, based on the  $k-\varepsilon$  model, the utilization of a spire as a vortex generator is effective only for near wake region ( $x_0=0\sim 13S$ ).

Based on Figure 10(b), same as the  $k-\varepsilon$  model, the  $SST k-\omega$  model also predicted a deeper BLH in the WS case by 400% at  $x_0=0.5S$ , which decreased down to the lowest point at  $x_0=20S$  and increased as the streamwise distance increased, compared to the WO case. However, unlike the  $k-\varepsilon$  model, the BLH of the WS case predicted by the  $SST k-\omega$  model is always higher than the WO case at any point in the streamwise direction. Hence, it can be concluded that, based on the  $SST k-\omega$  model prediction, it is effective to use a spire as a vortex generator because the BLH is deeper compared to that of the WO case throughout the numerical domain.

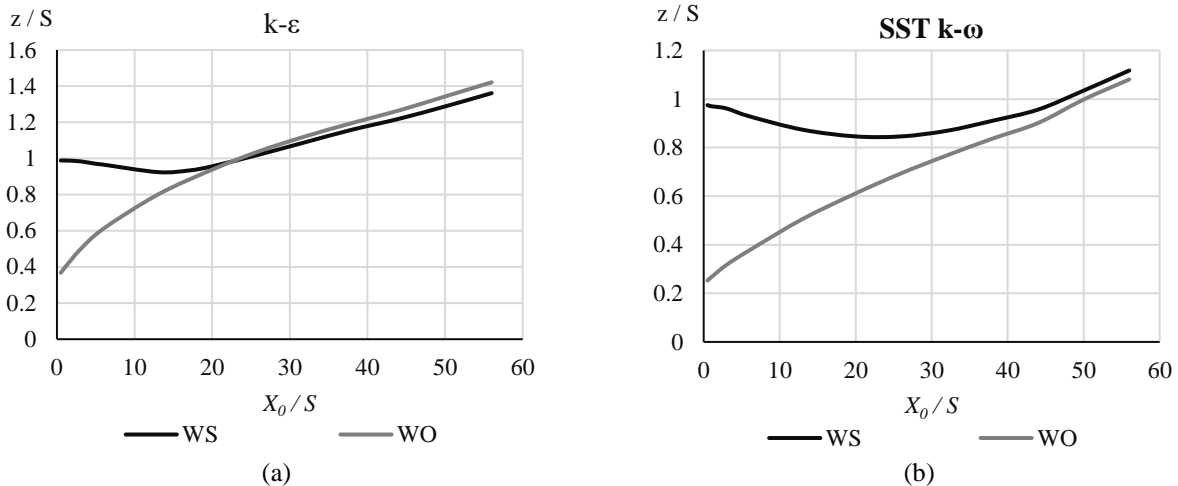


Figure 10. BLH development for both WO and WS cases using: (a)  $k-\varepsilon$  turbulence model and (b)  $SST k-\omega$  turbulence model

#### 4.0 CONCLUSIONS

The CFD simulations predicting the wake flow behind a single quarter-elliptic wedge spire (WS case) and the wake flow without a spire (WO case) were conducted. The mean vertical velocity profiles of the WO and WS cases are in good agreement with the previous wind tunnel experimental studies. Moreover, based on the comparison result of both turbulence models, it can be concluded that the  $k-\varepsilon$  overpredicts compared to the  $SST k-\omega$  turbulence model. Furthermore, the BLH predicted by each turbulence model was estimated. For the WO case, both turbulence models predicted that the BLH developed as the streamwise distance increased, which is in good agreement with the previous wind tunnel experimental studies. On the other hand, the BLH of the WS case was predicted to be rather irregular along with the streamwise direction. Both turbulence models predicted that the BLH of the WS case decreased at the near wake region ( $x_0=0\sim 6S$ ), created a minimum point, which is  $x_0=13S$  and  $x_0=20S$  the  $k-\varepsilon$  and  $SST k-\omega$  turbulence model respectively and increased along with the streamwise distance. This might be caused by the velocity deficit recovery that took place above the BLH region where the turbulence was relatively low. On top of that, the BLH of the WS case is always evidently greater than the WO case especially at the near wake region ( $x_0=0\sim 6S$ ) for both turbulence models. It can be assumed that the role of spires as vortex generators to increase the depth of the boundary layer is confirmed.

#### 5.0 ACKNOWLEDGMENTS

The authors gratefully acknowledge the research grant and financial support provided by the Ministry of Higher Education, MOHE (under the FRGS grant number: FRGS/1/2019/TK07/UMP/02/7 (RDU1901208) and Universiti Malaysia Pahang, UMP (under UMP grant number: RDU190375) also the MRS scholarship.

#### 6.0 REFERENCES

- [1] J. S. Yu, M. J. Emes, F. Ghanadi, M. Arjomandi, and R. Kelso, 'Experimental investigation of peak wind loads on tandem operating heliostats within an atmospheric boundary layer,' *Solar Energy*, vol. 183, pp. 248–259, 2019.
- [2] T. G. Ivanco, D. F. Keller, and J. L. Pinkerton, 'Investigation of atmospheric boundary-layer effects on launch-vehicle ground wind loads,' in *IEEE Aerospace Conference Proceedings*, 2020, pp. 1–20.
- [3] Abdollah Baghaei Daemei, 'Wind tunnel simulation on the pedestrian level and investigation of flow characteristics around buildings,' *Journal of Energy Management and Technology*, vol. 3, no. 1, pp. 58–68, 2019.
- [4] J. E. Cermak, 'Laboratory simulation of the atmospheric boundary layer,' *AIAA Journal*, vol. 9, no. 9, pp. 1746–1754, 1971.

- [5] S. Pengzhao, 'Simulation of atmospheric boundary layer in an open-loop wind tunnel using spire-roughness-element technique,' University of Windsor, *Master Thesis*, 2017.
- [6] N. A. Rahmat, A. Hagishima, and N. Ikegaya, 'An experimental study on aerodynamic interaction between a boundary layer generated by a smooth and rough wall and a wake behind a spire,' *Engineering Sciences Reports, Kyushu University*, vol. 37, no. 2, pp. 19–26, 2016.
- [7] N. A. Rahmat, A. Hagishima, N. Ikegaya, and J. Tanimoto, 'Experimental study on effect of spires on the lateral nonuniformity of mean flow in a wind tunnel,' *Evergreen*, vol. 5, no. 1, pp. 1–15, 2018.
- [8] V. Vikneshvaran, S. A. Zaki, N. A. Rahmat, M. S. Mat Ali, and F. Yakub, 'Evaluation of atmospheric boundary layer in open-loop boundary layer wind tunnel experiment,' *Journal of Advanced Research in Fluid Mechanics and Thermal Sciences*, vol. 72, no. 2, pp. 79–92, 2020.
- [9] H. Kozmar, 'Truncated vortex generators for part-depth wind-tunnel simulations of the atmospheric boundary layer flow,' *Journal of Wind Engineering and Industrial Aerodynamics*, vol. 99, no. 2–3, pp. 130–136, 2011.
- [10] S. Cao, A. Nishi, H. Kikugawa, and Y. Matsuda, 'Reproduction of wind velocity history in a multiple fan wind tunnel,' *Journal of Wind Engineering and Industrial Aerodynamics*, vol. 90, no. 12–15, pp. 1719–1729, 2002.
- [11] J. Counihan, 'An improved method of simulating an atmospheric boundary layer in a wind tunnel,' *Atmospheric Environment*, vol. 3, no. 2, pp. 197–214, 1969.
- [12] H. P. A. H. Irwin, 'The design of spires for wind simulation,' *Journal of Wind Engineering and Industrial Aerodynamics*, vol. 7, no. 3, pp. 361–366, 1981.
- [13] J. Armit and J. Counihan, 'The simulation of the atmospheric boundary layer in a wind tunnel,' *Atmospheric Environment*, vol. 2, no. 1, pp. 49–71, 1968.
- [14] A. Hagishima, J. Tanimoto, K. Nagayama, and S. Meno, 'Aerodynamic parameters of regular arrays of rectangular blocks with various geometries,' *Boundary-Layer Meteorology*, vol. 132, no. 2, pp. 315–337, 2009.
- [15] S. A. Zaki, A. Hagishima, J. Tanimoto, and N. Ikegaya, 'Aerodynamic parameters of urban building arrays with random geometries,' *Boundary-Layer Meteorology*, vol. 138, no. 1, pp. 99–120, 2011.
- [16] S. Ahmad Zaki, A. Hagishima, and J. Tanimoto, 'Experimental study of wind-induced ventilation in urban building of cube arrays with various layouts,' *Journal of Wind Engineering and Industrial Aerodynamics*, vol. 103, pp. 31–40, 2012.
- [17] H. Kozmar, D. Allori, G. Bartoli, and C. Borri, 'Complex terrain effects on wake characteristics of a parked wind turbine,' *Engineering Structures*, vol. 110, pp. 363–374, 2016.
- [18] H. Kozmar, D. Allori, G. Bartoli, and C. Borri, 'Wind characteristics in the wake of a non-rotating wind turbine close to a hill,' *Transactions of Famena*, vol. 43, no. 3, pp. 13–36, 2019.
- [19] I. Sho, 'Wind tunnel experiment on how mean flow heterogeneity affects turbulent statistics over a block array,' *Pusan National University*, 2016.
- [20] Vikneshvaran, S. A. Zaki, N. A. Rahmat, M. S. M. Ali, and F. Yakub, 'Evaluation of atmospheric boundary layer in open-loop boundary layer wind tunnel experiment,' *Journal of Advanced Research in Fluid Mechanics and Thermal Sciences*, vol. 72, no. 72, pp. 79–92, 2020.
- [21] H. Kozmar, 'Scale effects in wind tunnel modeling of an urban atmospheric boundary layer,' *Theoretical and Applied Climatology*, vol. 100, no. 1, pp. 153–162, 2010.
- [22] J. Nagawkar, S. Ghosh, R. Kataria, A. Nashit, and A. Deora, 'Effect of sky scrapers on natural ventilation patterns and human comfort index in low-rise buildings - a CFD analysis over central Mumbai,' *ARPN Journal of Engineering and Applied Sciences*, vol. 9, no. 3, pp. 293–295, 2014.
- [23] Z. Harun, E. Reda, and S. Abdullah, 'Large eddy simulation of the wind flow over skyscrapers,' *Recent Advances in Mechanics and Mechanical Engineering*, vol. 15, pp. 72–79, 2015.
- [24] I. A. M. Gad, 'Spalart-allmaras turbulence model validation for flow around skyscraper model,' *Egyptian Journal for Engineering Sciences and Technology*, vol. 14, no. 1, pp. 130–143, 2011.
- [25] D. Mohotti, K. Wijesooriya, and D. Dias-da-Costa, 'Comparison of Reynolds Averaging Navier-Stokes (RANS) turbulent models in predicting wind pressure on tall buildings,' *Journal of Building Engineering*, vol. 21, pp. 1–17, 2019.
- [26] A. F. Mohammad, S. A. Zaki, S. S. Suhaimi, M. Sukri, and M. Ali, 'Preliminary CFD investigation of wind velocities in the staggered arrays of flat- and gable-roofed buildings,' *Malaysia-Japan Joint International Conference (MJJIC), Kuala Lumpur, Malaysia*, 2016.
- [27] F. Juretić and H. Kozmar, 'Computational modeling of the neutrally stratified atmospheric boundary layer flow using the standard k- $\epsilon$  turbulence model,' *Journal of Wind Engineering and Industrial Aerodynamics*, vol. 115, pp. 112–120, 2013.

- [28] F. Juretić and H. Kozmar, 'Computational modeling of the atmospheric boundary layer using various two-equation turbulence models,' *Wind and Structures*, vol. 19, no. 6, pp. 687–708, 2014.
- [29] H. Kozmar, 'Surface pressure on a cubic building exerted by conical vortices,' *Journal of Fluids and Structures*, vol. 92, p. 102801, 2020.
- [30] H. Kozmar and B. Laschka, 'Wind-tunnel modeling of wind loads on structures using truncated vortex generators,' *Journal of Fluids and Structures*, vol. 87, pp. 334–353, 2019.
- [31] D. D. Apsley and M. A. Leschziner, 'Advanced turbulence modelling of separated flow in a diffuser,' *Flow, Turbulence and Combustion*, vol. 63, no. 1, pp. 81–112, 2000.
- [32] Saffman PG, 'A model for inhomogeneous turbulent flow,' *Proceedings of the Royal Society of London A Mathematical and Physical Sciences*, vol. 317, no. 1530, pp. 417–433, 1970.
- [33] S. Murakami, 'Comparison of various turbulence models applied to a bluff body,' *Journal of Wind Engineering and Industrial Aerodynamics*, vol. 46–47, pp. 21–36, 1993.
- [34] Y. Tominaga and T. Stathopoulos, 'CFD simulation of near-field pollutant dispersion in the urban environment: A review of current modeling techniques,' *Atmospheric Environment*, vol. 79, pp. 716–730, 2013.
- [35] OpenFOAM, 'User Guide: k-epsilon – OpenFOAM V2006'. p. 6, 2017.
- [36] B. E. Launder and B. I. Sharma, 'Application of the energy-dissipation model of turbulence to the calculation of flow near a spinning disc,' *Letters in Heat and Mass Transfer*, vol. 1, no. 2, pp. 131–137, 1974.
- [37] F. R. Menter, 'Influence of freestream values on k- $\omega$  turbulence model predictions,' *AIAA Journal.*, vol. 30, no. 6, pp. 1657–1659, 1992.